First Demonstration of a Low Cost/Customizable Chip Level 3D Printed Microjet Hotspot-Targeted Cooler for High Power Applications

T.-W. Wei[1,2], H. Oprins[1], V. Cherman[1], I. De Wolf[1,3], E. Beyne[1], M. Baelmans[2]
[1]imec, Leuven, Belgium, [2]Dept. Mech. Eng. KU Leuven, Leuven, Belgium,
[3]Dept. Materials Eng. KU Leuven, Leuven, Belgium
email: tiwei.wei@imec.be

***Abstract*—This work presents the modeling, design, demonstrator fabrication and experimental characterization of a customized chip level direct liquid impingement jet cooler for hotspot cooling, fabricated with high-resolution stereolithography technology. The study, using a dedicated thermal test vehicle, demonstrates that 3D printing enables the design and low-cost fabrication of high-performance impingement coolers matching hotspot power dissipation patterns. The hotspot targeted cooler can improve the thermal resistance by 36% compared with full nozzle array cooling for the same flow rate.**

I. INTRODUCTION

With the increasing trend of the heat flux as well as the scaling down of the transistor size, thermal management becomes more and more challenging due to the performance and reliability degradation with elevating chip temperature. For practical microprocessor or power electronic devices, the heat flux on the chip is mostly non-uniform showing various hotspot patterns with different localized heat flux values. Therefore, controlling the maximum temperature of the hotspot always determines the thermal design in the thermal management of electronic devices and packages [1]. On the other hand, the control of the temperature uniformity across the whole chip is also important since a larger temperature gradient can increase the thermal stress and reduce the electronic reliability and circuit imbalances in devices [2].

Single phase liquid cooling has been regarded as an effective and practical solution for high power electronics and high-performance systems. In general, the research studies regarding the liquid cooling of the chip temperature are mostly focused on the maximum temperature reduction and chip temperature uniformity. However, the hotspot management on chip level is very challenging due to the complexity of the cooler fabrication. In literature [2,3], an extensive overview of the hotspot target cooling techniques is discussed. Most of the cooling solutions are based on Si processing, including hotspot-targeted embedded liquid cooling by adapting the channel density with the hotspot [2], micro-gaps with variable pin fin clustering [4], thermoelectric cooling (TEC) [5], alternating current electrothermal flow (ACET) cooling [3] and electrowetting droplet on hotspot [6]. However, the drawbacks of these techniques are low energy conversion efficiency, low heat flux pumping capacities, high cost and introduction of additional thermal resistances in the heat flow path.

Polymer based bare die liquid micro-jet impingement cooling is an efficient cooling technique for high power electronics, especially for hotspot management. The advantage of microjet cooling is that it can directly target the hotspot by placing jet nozzles on top of the hotspot. Previously [7], we have first introduced a chip level 3D-shaped polymer cooler with sub-mm nozzle diameters fabricated using mechanical micromachining. A cross section of this cooling concept is shown in Fig. 1. The performance benchmarking study shows that low cost polymer based 4×4 microjet coolers can achieve similar thermal performance at lower required pumping power than much more expensive silicon and ceramic based microjet coolers [7].

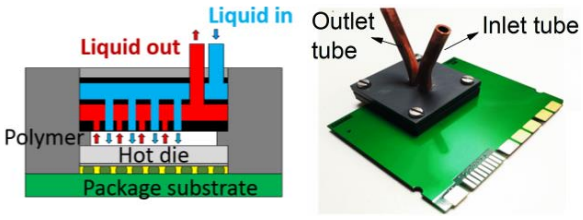

(a) (b)

Figure 1. Cross section of the bare die impingement jet cooling concept (a) and (b) micromachined cooler for the 8x8 mm^2 chip in the 14x14 mm^2 BGA package [7].

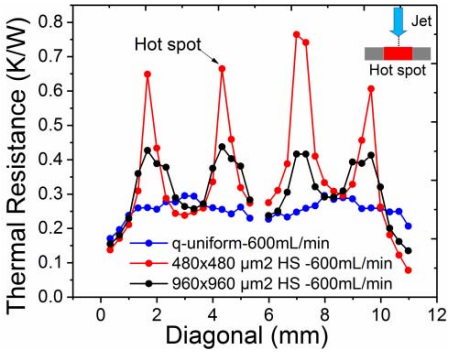

Figure 2. Measurement results with aligned nozzles and hotspot locations for different hotspot area [8].

Hotspot measurements for this 4×4 micromachined cooler, assembled on the thermal chip show that the temperature peak is significantly higher for hotspot power dissipation, even though impingement cooling achieves a very good cooling performance [8], as shown in Fig.2, Therefore, a customized hotspot targeted cooling design is needed for high performance chips with non-uniform power distribution. The main idea of hotspot targeted cooling is to focus the cooling solution, at the location where it is needed. In terms of impingement cooling, this means to concentrate the impinging

2377-5726/19/$31.00 ©2019 IEEE
DOI 10.1109/ECTC.2019.00027

of the liquid coolant and the high power areas in the chip. This cooling concept is illustrated in Fig.3. For the hotspot targeted impingement cooler, the location of the inlet nozzles that eject the coolant onto the chip should be aligned with the location of the hotspot.

As shown in the concept, isolated inlet nozzles have to be built to target at the hotspot. However, the use of micromachining techniques to fabricate such a cooler increases the manufacturing complexity since the nozzles targeted at the hotspot have to be drilled one after one and also the micro-milling process for the inlet and outlet plenum that connects all inlets and outlets becomes challenging. And also, the cooler has to be fabricated with different parts by micromachining. The assembly of different parts increases the risks of the water leakage. Therefore, we introduced the use of additive manufacturing to fabricate polymer impingement coolers to increase the design options for polymer coolers for more complex geometries [9]. Additive manufacturing enables to use low cost materials for the cooler fabrication, to print the whole geometry in one piece and to customize the design to match nozzle array to the chip power map. The details of the internal fluidic channels and inlet/outlet nozzles for the 3D printed 4x4 jet array cooler are shown in Fig.4.

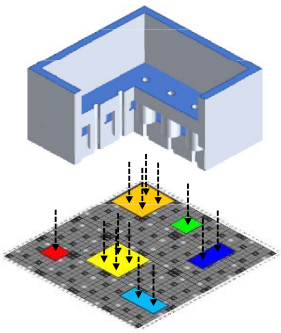

Figure 3. Concept of hotspot targeted liquid impingement cooling.

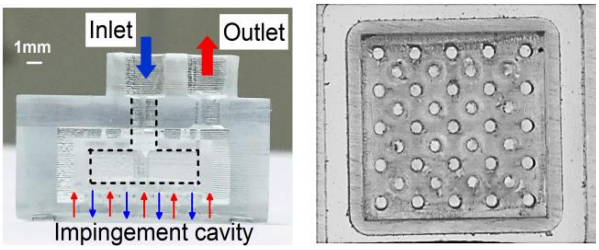

(a) (b)

Figure 4. Fabrication of the 3D printed cooler [9]. Detail of the channels in cross-section of the cooler (a); bottom view of the nozzle plate with inlet/outlet nozzles (b).

In this paper, we present the design, fabrication and experimental characterization of a highly efficient customizable and low cost hotspot targeted cooling solution for high power electronics fabricated using additive manufacturing. In order to evaluate the thermal performance, the printed cooler is assembled to a 8×8 mm^2 thermal test chip [10] with an array of 32×32 temperature sensors and programmable heat dissipation patterns. The possible power dissipation patterns range from customized hotspot patterns to quasi-uniform power dissipation on the chip area.

The first section of the paper (Section 2) presents the manufacturing tolerance analysis with the 3D printed cooler, including the impact of the nozzle diameter variation, nozzle angle deviation, and the nozzle-to-chip distance deviations. Next in in Section 3, the design and fabrication of the hotspot targeted cooler demonstrators with two different test cases are introduced in detail. Then in section 4, the thermal performance between the uniform nozzle array cooling and hotspot targeted cooling are characterized and compared based on the advanced thermal test chips. Finally, the CFD full cooler level model is validated with experimental measurements. Based on the validated CFD model, the velocity and pressure information inside the hotspot targeted cooler are extracted. Moreover, the thermal-hydraulic trade-off analysis is summarized based on the system considerations for constant flow rate, pressure drop or pumping power.

II. MANUFATURING TOLERANCE ANALYSIS

A. Manufacturbaility analysis of SLA

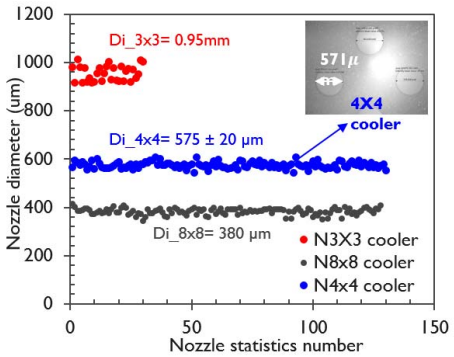

Figure 5. Nozzle diameter variation measurements with 3×3, 4×4 and 8×8 array cooler.

First, the fabrication tolerance and the deviation of the printed geometry from the nominal design are evaluated for the used high-resolution Stereolithography (SLA) technology. Microscopy is used to measure the nozzle diameter. Fig. 5 shows the measurement results of the printed nozzles diameters for different types of coolers (3×3, 4×4 and 8×8 nozzle arrays) that have been designed and fabricated for the 8 × 8 mm^2 test chip. The deviation between the measured printed nozzle (575 μm ± 10 μm) and the nominal design value of 600 μm is only 5% The measurements of the printed nozzle diameters for different cooler nozzle arrays, show that 3D printing is capable of producing the coolers with a small nominal diameter of 300 μm for the 8×8 array on the 8×8 mm^2 chip area, with high reproducibility. The unit cooling cell is 1×1 mm^2 with a nozzle diameter ratio of 0.3. This nozzle diameter ratio is defined as the nozzle diameter divide by unit cell length.

B. Impact of nozzle diameter deviation

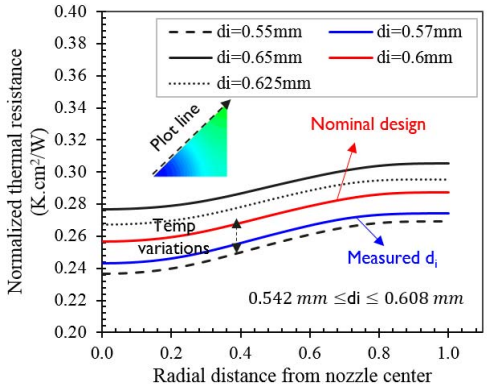

Figure 6. Impact of the nozzle diameter deviations on the temperature distributions for 2×2 mm^2 cooling unit cell area with nominal design nozzle diameter of 600 µm. (flow rate = 600 ml/min, Q = 50 W).

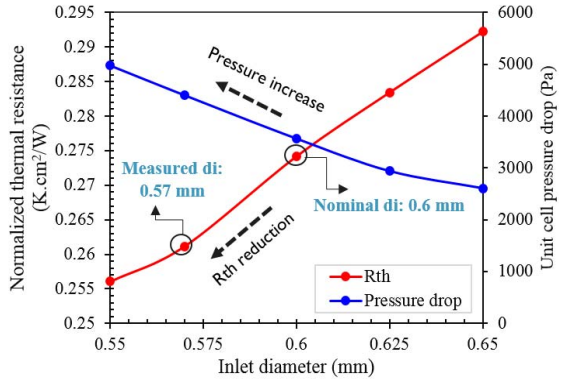

Figure 7. Impact of the inlet/outlet nozzle diameter on the averaged chip temperature and pressure drop for 2×2 mm^2 cooling unit cell area with nominal design nozzle diameter of 600 µm. (flow rate =600 ml/min, Q = 50 W).

In order to understand the impact of the 3D printing fabrication tolerance on the cooler thermal/hydraulic performance, the impact for a nozzle geometry of a 4×4 cooler with cooling unit cell area of 2×2 mm^2, and a nominal nozzle diameter of 600 µm, is investigated numerically. A unit cell computation fluid dynamics (CFD) modeling approach is used to assess the impact of the geometry deviation on the temperature and pressure drop based on the 4×4 array cooler. The used CFD software package is ANSYS Fluent. The deviation between the measured printed nozzle (575 µm ± 20 µm) and the nominal design value of 600 µm is only 5% for 4×4 array cooler. Fig.6 shows that the normalized thermal resistance will drop down for a decrease of the nozzle diameter at a constant flow rate. The reason is that the inlet nozzle velocity will increase due to the reduction of the nozzle diameter for the fixed flow rate. For the impingement jet cooling, the chip temperature is dominated by the stagnation point where the inlet jet nozzles are targeted. The stagnation temperature in the temperature profile shows about 7.7% variation for the nozzle diameter ranging from 0.55 mm to 0.6 mm for the 4×4 cooler. The reduction of the nozzle diameter can reduce the chip temperature, however, at the expense of a higher pressure drop. The thermal and hydraulic comparison between the nominal design and actual measured values are illustrated in Fig.7. The modeling study shows that the nozzle diameter deviation of 5% at flow rate of 600 ml/min results only in a 4.7% reduction for the averaged chip temperature and 23% higher for the pressure drop.

C. Impact of nozzle angle deviation

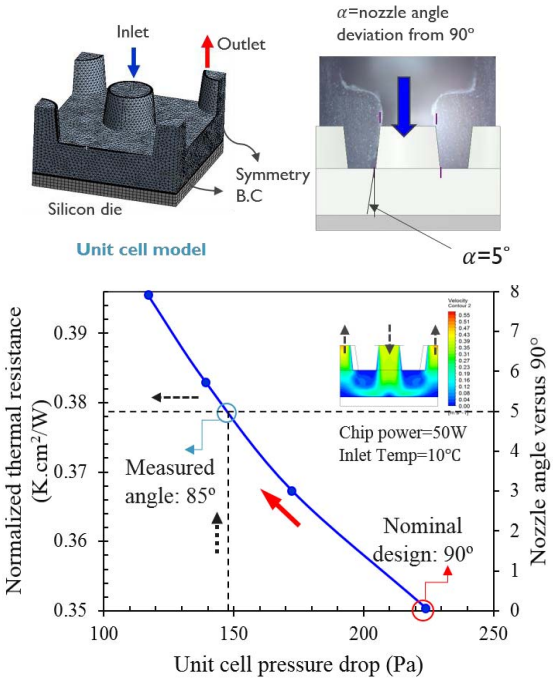

Figure 8. Unit cell modeling study on the impact of nozzle angle on the thermal and hydraulic performance for 2×2 mm^2 cooling unit cell area with nominal design nozzle diameter of 600 µm. (flow rate =300ml/min, Q=50W)

The cross-section pictures of the printed cooler show that the nozzle shapes are slightly tapered instead of straight. The tapered nozzle can reduce the cooling performance due to the less concentrated flow targeted at the stagnation point, resulting in a higher local chip temperature. At the other hand, the tapered inlet nozzle and outlet nozzle shape can help to reduce the pressure drop. As shown in Fig.8, the modeling study shows that a nozzle diameter deviation of 5º (85º instead of 90º) only results in a 8% difference for the averaged chip temperature but caused a 34.2% reduction for the local pressure drop on the unit cell level.

D. Impact of nozzle-to-chip distance deviation

In order to define the deviation of the nozzle-to-chip distance *H*, the groove depth, the thickness of the O-ring and the fabrication tolerance of the cavity height should be

considered. For the cavity height and groove, the actual depth is about 0.65 mm compared to the nominal design value of 0.6 mm. The groove at the cooler bottom is designed for the O-ring assembly. The thickness of the O-ring is 1 mm, which will be placed on the organic substrate. The chip thickness is 0.2 mm. The thickness of the micro-bump used to connect the thermal test chip and organic substrate is 0.02 mm. Taking account into the O-ring thickness without compression, the distance between the nozzles and chip cooling surface is 0.78 mm. Therefore, the nozzle-to-chip backside distance variation is expected to between 0.6 mm to 0.8 mm.

The impact of the nozzle-to-chip distance above the chip cooling surface is shown in Fig. 9. The modeling study shows that the impact on the thermal resistance is negligible beyond 0.6 mm while the impact on the cooler pressure drop will result in a difference of 1.1 % between the range of 0.6 mm and 0.8 mm. Therefore, the nozzle-to-chip distance variations shows less impact on the chip averaged temperature when the nozzle-to-chip distance ratio is above H/L > 0.25.

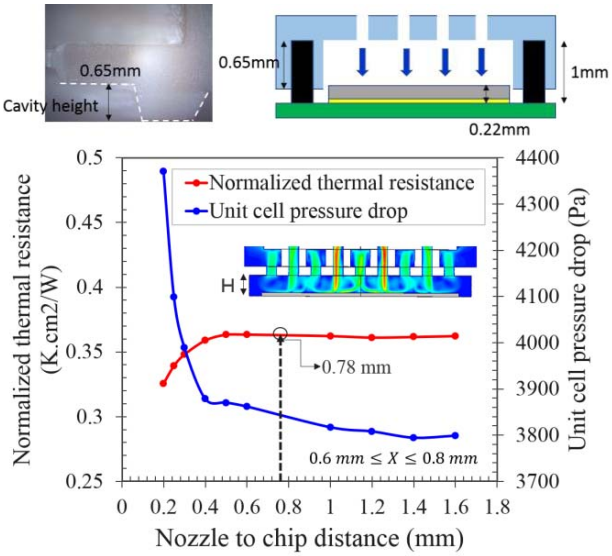

Figure 9. Impact of the nozzle-to-chip distance variations for the for 2×2 mm^2 cooling unit cell area with nominal design nozzle diameter of 600 µm. (flow rate =300ml/min, Q=50W).

III. 3D PRINTED HOTSPOT COOLER DEMONSTRATOR

A. Thermal test chip with HS

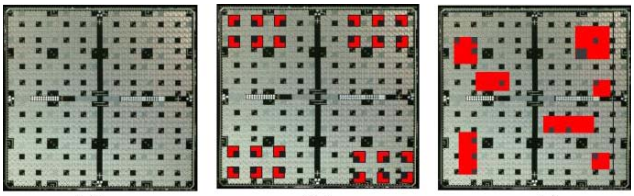

(a) (b) (c)

Figure 10. Test cases for the hotspot cooling: a) reference case with quasi-uniform cooling; b) test case 1 with regular pattern; c) test case 2 with various hotspot size;

In order to investigate the hotspot targeted cooling, two hotspot case studies have been defined: test case 1: regular hotspot pattern and test case 2: various hotspot sizes. These power dissipation maps are generated with the programmable test chip and are all shown in Fig.10. For the thermal test chip, the chip area is 8×8 mm^2 while the chip heated area is 75% of the chip surface. The thermal test chip is divided into a 32 × 32 array of 240 × 240 µm^2 square cells with additional peripheral circuits with I/O and control cells in the central cross of the chip [9]. There are 32×32 array of 'thermal pixel' cells with a diode as temperature sensors. The sensor temperature sensitivity is calibrated as -1.55 mV/ºC. Moreover, there are 832 cells indicated as 'heater cells' within the 32 × 32 array. The heater cells are programmable since each cell is individually controlled by a local transistor. The single heater cell is equipped with two 200 × 100 µm2 metal meander heaters in the back-end of line (BEOL). The maximal measured power for the single heater cell is 47.6mW at 1V, resulting in a maximal heat flux per cell about 82.6 W/cm^2.

For test case 1 with the regular hotspot pattern, there are 72 heater cells turned on. The total heater area is 4.15 mm^2, with a total measured chip power of 4.1 W. For test case 2 with various hotspot size pattern, the total number of the activated heater cells is 127, with a corresponding heater area of 7.32 mm^2 and a total measured heat power 5.5 W. These two different hotspot patterns are designed to mimic hotspot scenarios in power electronic devices.

B. HS cooler design

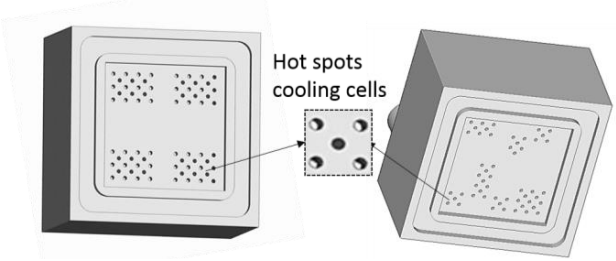

(a) (b)

Figure 11. Designs of the hotspot cooler with 300 µm nozzles diameter: regular pattern (a) and various hotspot sizes (b) with 1×1 mm^2 cooling unit cell area.

Based on the manufacturing capabilities of the 3D printing technology, two different hotspot coolers based on the geometry of a cooling cell area of 1×1 mm^2 have been designed to match with the two hotspot test cases shown in Fig.10 (b) and (c). For the 8×8 mm^2 chips, this means that the nozzle array is based on the 8×8 array of cooling cells. In the hotspot targeted cooler designs, the inlet nozzles are kept at the locations of the hotspot, and removed at the locations where not power generation is present. Fig.11 shows the design details of the dedicated hotspot cooler for the two test cases with a nominal nozzle diameter of 300 µm. The design software used in this study is VariCAD. Moreover, the internal fluidic channels are illustrated in Fig.12, showing the flow directions inside the cooler. The nozzles within the

cooling unit cells are designed specifically and aligned with the hotspot while no designed cooling cells are in the "cold region".

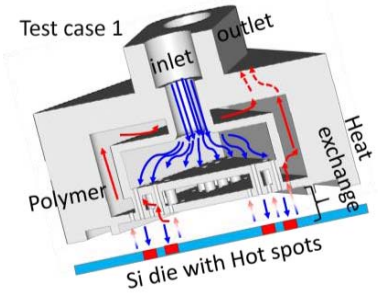

Figure 12. Interior view of 3D hotspot targeted cooler for the regular hotspot pattern.

C. Fabrication of 3D printed cooler

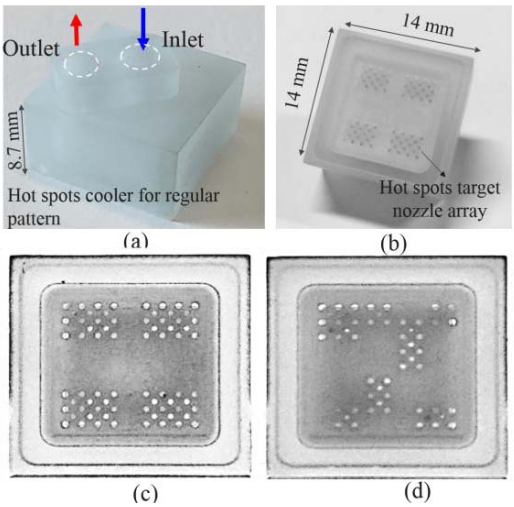

Figure 13. Fabricated demonstrators for the hotspot targeted cooler: a) top view and (b) bottom view of the printed cooler; c) and d) with bottom view of fabricated nozzle patterns.

The objective is to compare uniform liquid impingement cooling over the whole chip surface with dedicated cooling only at locations where it is needed. Fig. 13 shows the printed coolers for the two hotspot test cases. The total cooler size is 14 mm×14 mm×8.7 mm matched with the package substrate size. The bottom view of the two hotspot targeted coolers reveals the location of the corresponding to the hotspot patterns of the test cases. The groove for the placement of O-ring can be also seen in the figure.

IV. COOLER THERMAL CHARACTERIZATION

The dedicaed hotspot cooler is assembled on the advanced thermal test chip with programmable heater cells and 32×32 array of temperature sensors, illustrated in Fig.14(b). The O-ring is placed inside the groove to seal the cooler shown in Fig.14(a). The hotspot cooler with test board is finally assembled into the liquid flow loop with dedicated pressure sensor, heat exchanger and flow rate controller. The inlet temperature is set as 10 ˚C. The chip temperature sensors allow absolute temperature measurements with an accuracy of ± 2-3 ºC.

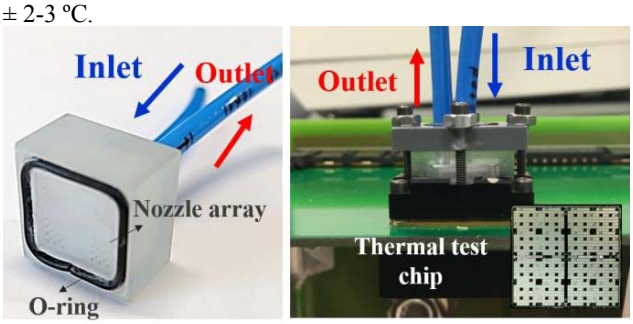

Figure 14. Cooler assembly: (a) hotspot targered cooler for regular pattern with O-ring placement; (b) assembly of the cooler on the thermal test chip and test PCB board.

For the characterization of the hotspot targeted coolers, the measured temperature maps for both coolers have been compared to the temperature maps obtained with the full array coolers at the same flow rate for the corresponding hotspot power dissipation maps, as shown in Fig.15. Fig. 16 shows the temperature profiles for the array cooler and the hotspot targeted cooler for diagonal/vertical line scan across the measured temperature maps of Fig. 15. These temperature measurements show a peak temperature reduction of 16% shown in Fig.16(a) and 24% shown in Fig.16(b) at a flow rate of 900 mL/min/cm^2 compared to the full array cooler for the targeted hotspot coolers of test case 1 and test case 2 respectively.

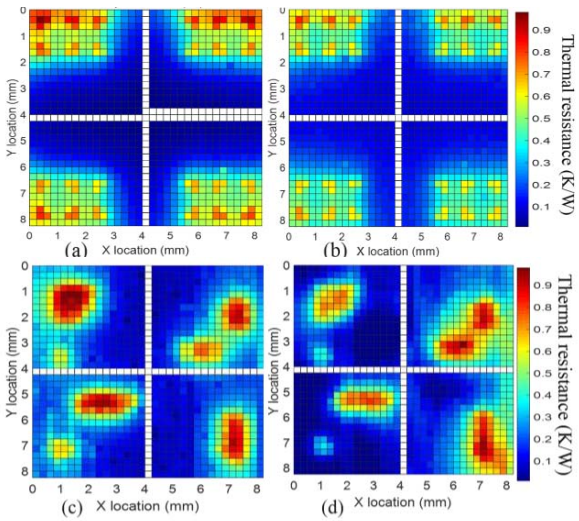

Figure 15 Chip temperature distribution measurements for (a) nozzle array uniform cooling and (b) HS targeted cooling for regular pattern at the flow rate of 600ml/min; Measurements of (c) nozzle array uniform cooling and (d) HS target cooling for test case 2 at same flow rate of 1000 ml/min.

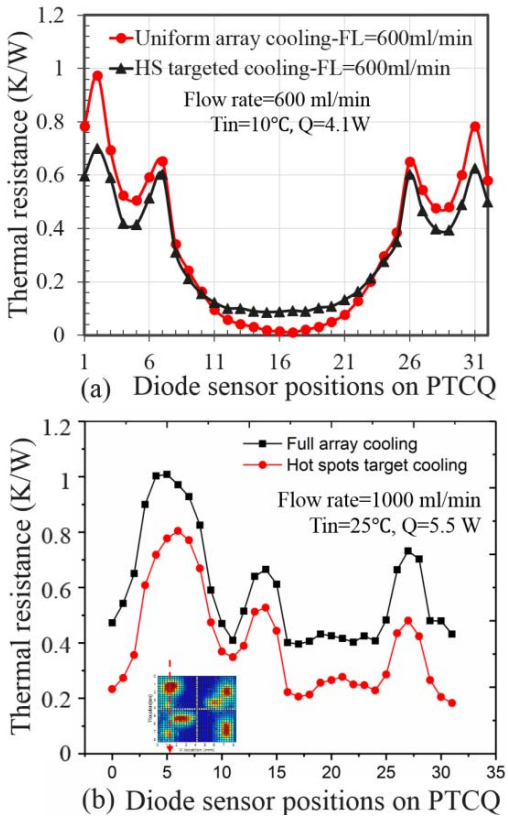

Figure 16. Experimental measurements of HS cooling with (a) test case 1 at the flow rate of 600 ml/min and (b) test case 2 at the flow rate of 1000 ml/min.

V. SYSTEM LEVEL MODELING ANALYSIS

A. Full cooler level model

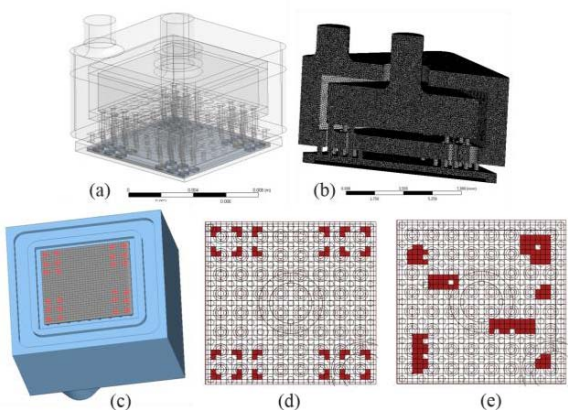

Figure 17 Full cooler level CFD model: (a) transparent view of the cooler geometry; (b) cross section of the mesh of test case 1; (c) indication of the thermal test die on the full cooler; (d) detailed heater cells of test case 1 and test case 2.

In order to extract more detailed temperature, velocity and pressure drop information inside the dedicated cooler, a full cooler level CFD model is built including the details of the hotspot heater cells, as shown in Fig.17. The element size for the fluid domain is set as 0.12 mm while the meshing size is 0.04 mm for the solid domain in order to include sufficient detail of the heater cells. The boundary layer is defined as the impingement jet region, which is the interface between the liquid and chip surface. The first layer thickness of the boundary layer is set as 1e-3 mm with 10 layers above fluid/solid interface, with layer growth rate 1.2. The total number of elements is 1.6M. In order to capture the temperature map of the hotspot cooling, a high level of details in the thermal model of the heaters is needed for the high heat removal rates obtained in high cooling performance impingement cooler [8].

B. CFD Model validation

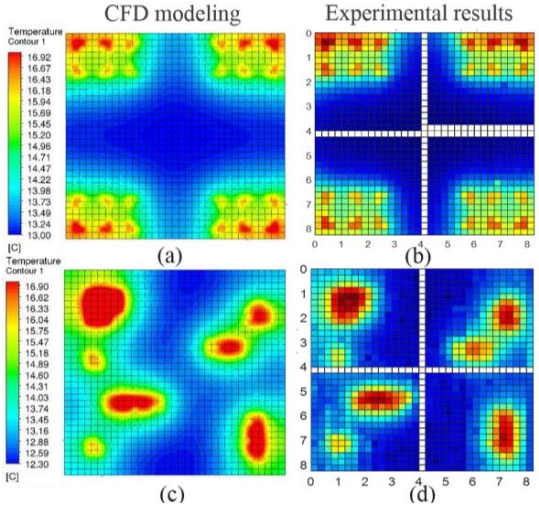

Figure 18. Temperature map distribution of CFD modleing versus experimental measurement: test case 1 (a) with CFD modeling and b) experimental results (flow rate =600 ml/min, Q=4.1W); test case 2 with (c) CFD modeling and (d) experimental results (flow rate =600 ml/min, Q=5.5 W).

As illustrated in Fig.18, the temperature distribution comparisons between the full cooler level CFD modeling and experimental results for the regular pattern are illustrated. For the test case 1, the comparisons between the experiments and CFD modeling results show that the averaged chip temperature is less than 2.5% difference compared with the experimental results with uniform nozzle array cooling, while the difference is 8.5% for hotspot cooling. For the averaged chip temperature in the test case 2, the comparison shows about 18.3% difference comparing with the experimental data for uniform nozzle array cooling. The asymmetrical temperature map shown in Fig.19(a) and (b) is due to the placement of the outlet tube connector, which is located at the one side of the cooler.

The comparison of hotspot cooling with various hotspot size in Fig.19(c) also indicates that the full CFD cooler level model can capture the major trends of the experimental results. In general, the modeling curve for HS array cooling shows good agreement with the experimental curve. Based on the acceptable errors of the full CFD cooler model comparing

with experimental data, the CFD model with hotspot cooler is successfully validated. This means that we can use the validated CFD model for future design improvements of the printed cooler and to assess the trade-off between the thermal performance improvement and the pressure drop penalty in the hotspot targeted cooler.

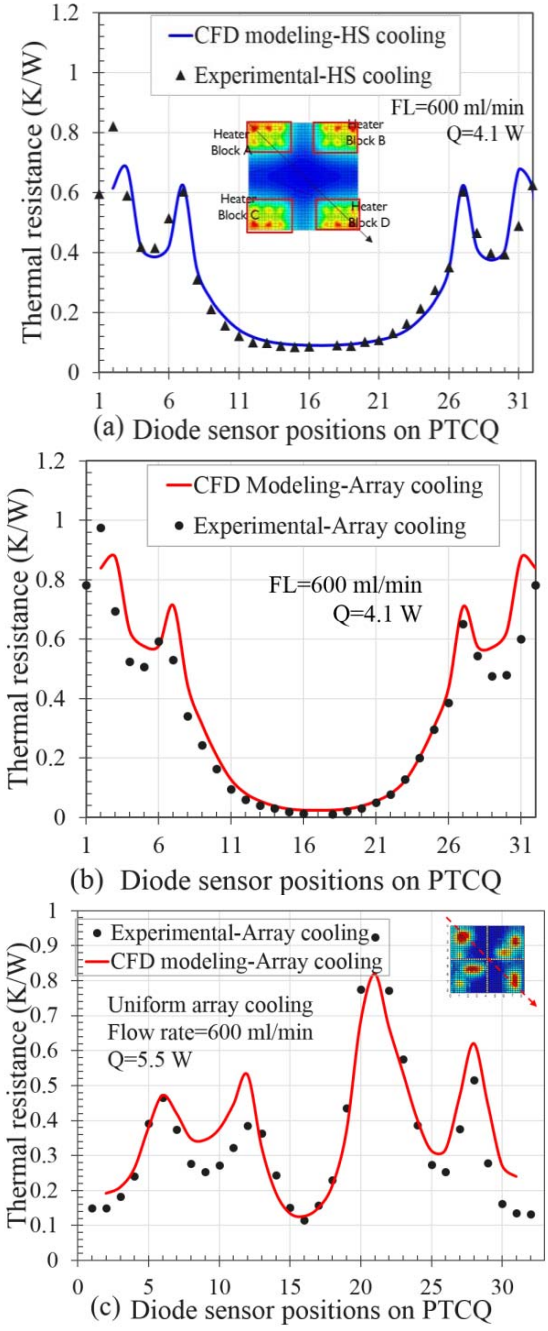

Figure 19. Experimental CFD model validation for cooler of test case 1 with (a) hotspot targeted cooling and (b) nozzle array uniform cooling; (c) experimental validation for test case 2 with nozzle array uniform cooling.

C. *Hydraulic performance analysis*

From the above experiments and modeling studies, we can see that the hotspot target cooling can achieve lower temperature by concentrating the coolant, but higher pressure is required to push the same flow rate through smaller number of nozzles. Therefore, more information about the nozzle velocity and pressure are needed. In the following section, the validated CFD model is first used to extract the hydraulic behavior inside the coolers. The flow streamlines inside the hotspot cooler for test case 1 and test case 2 are both shown in Fig.20. The flow streamline inside the distributor shows more flow recirculation for the hotspot targeted cooling since the flow is concentrated into the reduced number of inlet nozzles.

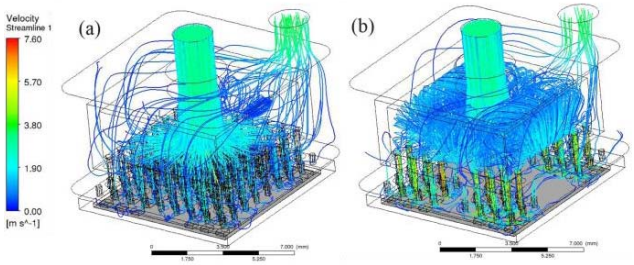

Figure 20. Flow streamlines inside the cooler for (a) uniform nozzle array cooling and (b) hotspot targeted cooling. (flow rate =600ml/min)

Moreover, the validated CFD model is also used to extract the internal velocity and pressure information for different nozzle arrays as shown in Fig.21. The pressure drop between inlet and outlet of the cooler for the nozzle array uniform cooling with regular pattern is 0.16 bar while the pressure drop is 0.57 bar for hotspot targeted cooler. The comparison indicates that the pressure drop increases by a factor of 3.56X for the same flow rate. Moreover, the flow distribution for every inlet nozzle is shown in Fig.21 (c). The velocity is plotted across the nozzle plate region by covering the inlet/outlet velocity. The flow distribution for full array cooler shows about 57% maximum deviation in the center while the maximum deviation is 22% in other regions compared with the theoretical velocity of 2.2 m/s. The large deviation in the center is due to the inlet impinging flow coming from the top. For the hotspot cooler, the velocity for the nozzles are with maximum difference of 13.5% comparing with theoretical velocity value of 5.9 m/s.

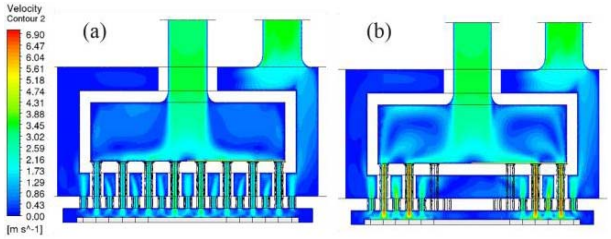

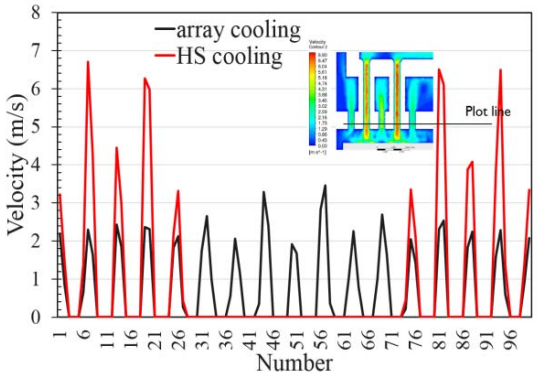

Figure 21. Velocity information extractions for regular HS pattern: cross section of the velocity distribution for (a) nozzle array cooling and (b) hotspot targeted cooling; (c) inlet velocity profile comparison.

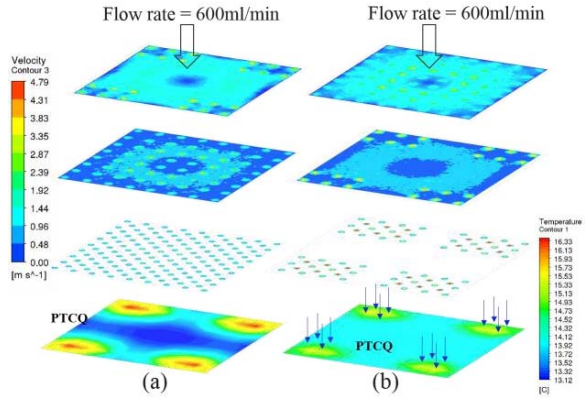

Figure 22 Flow and thermal interactions with (a) nozzle array cooling and (b) hotspot targeted cooling.

As shown in the flow and thermal interaction analysis in Fig.22, we can see that, hotspot targeted cooler with locally high flow rate can locally reduce the HS temperature with the constant total flow rate.

D. Thermal – hydraulic trade-off analysis

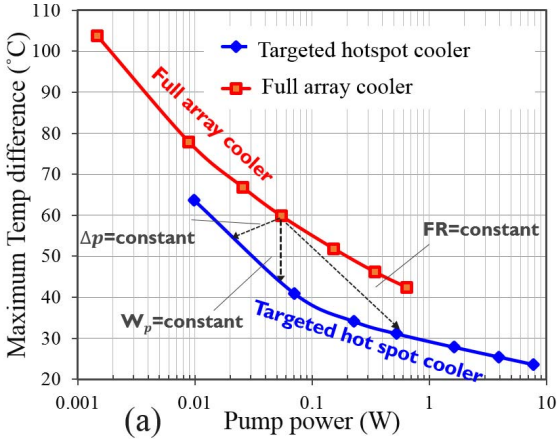

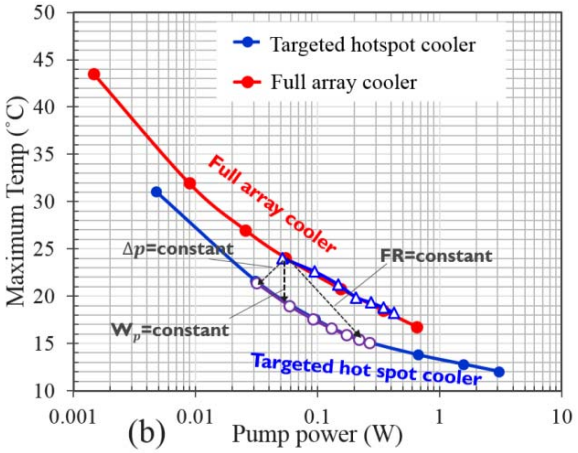

Figure 23. Thermal/hydraulic performance trade-off comparison between the hotspot cooler and the full array cooler for (a) test case 1 and (b) test case 2.

In the last section, the comparison between the hotspot targeted cooler (test case 1) and the full array cooler is shown in Fig.23(a). The performance of the two coolers is shown as curves in terms of the hotspot peak temperature ΔT_{max} and the required pumping power for a range of low rates. A lower position of the curve, closer to the origin, corresponds to a better performance. The performance of the coolers is now compared for different constraints [11]:

1. Same pressure drop over the cooler
2. Same flow rate
3. Same pumping power

For the same pressure drop of 10 kPa, the ΔT_{max} can drop by a factor of 1.08 for the hotspot targeted cooler compared to the full array cooler, but it would use 2.5x less flow rate and pumping power. For the same flow rate at 100 ml/min, the ΔT_{max} can reduce by a factor of 2, but it requires 10x larger pressure drop; For the same pumping power at 0.05W, the ΔT_{max} drops by 35% compared to the full array cooler.

The comparison for test case 2 is shown in Fig.23(b). For the same pressure drop at 10 kPa, the ΔT_{max} can drop by a factor of 1.1, but with less flow rate; For the same flow rate at 100ml/min, the ΔT_{max} can reduce by 1.54x, but with larger pressure drop; For the same pump power at 0.05W, the ΔT_{max} drop by 1.36x. In general, for all considerations, the hotspot cooler curve shown in blue is below the full array cooler curve (in red), indicating that the hotspot targeted cooling is more energy efficient compared with the full array cooler for specific hotspot patterns.

CONCLUSIONS

This work demonstrates the hotspot targeted cooler for high power devices with localized high heat flux regions, for the first time using 3D printing, which enables the fabrication of a matching design of the cooler nozzle array to the power map, and at the same time offers a huge reduction in the cooler size, matching the footprint of the power electronics

packaging. Two types of hotspot cooler with a small nominal diameter of 300 μm for a cooling unit cell area of 1×1 mm^2 are demonstrated with high reproducibility. The fabrication tolerance has been assessed and its impact on the thermal and hydraulic performance has been evaluated by using unit cell CFD models. The modeling study shows that there is a benefit with respect to significant pressure drop reduction due to the slightly tapered fabricated nozzle wall while this results in a slight reduction of thermal performance. The thermal impact of the nozzle-to-chip distance variation is negligible for cavity heights with H/L > 0.25 due to the cooling saturation.

The hotspot cooling experimental measurements show a peak temperature reduction of 16% and 24% at a flow rate of 900 mL/min/cm^2 compared to the full array cooler for the targeted hotspot coolers of test case 1 and test case 2 respectively. Moreover, the experimentally validated full cooler level CFD models for both test cases are used to investigate the thermo-hydraulic behavior of the cooler for different flow constraint conditions. The trade-off charts between the maximum temperature difference and required pumping power prove that the hotspot targeted cooler exhibits a more energy efficiency cooling performance compared with the uniform nozzle array cooler for the hotspot test cases for all considered comparison constraints.

ACKNOWLEDGMENTS

This work was performed as part of the imec Industrial Affiliation Program on 3D System Integration and has been strongly supported by the imec partners and the imec Reliability, Electrical testing, Modeling and 3D technology teams.

REFERENCES

[1] Avram Bar-Cohen, “On-chip thermal management and Hotspot remediation, Nano-Bio- Electronic”, Photonic and MEMS Packaging. 2009, pp 349-429.

[2] C S Sharma, “Energy efficient hotspot-targeted embedded liquid cooling of electronics”, Applied Energy, Volume 138 2015, pp. 414-422.

[3] Golak Kunti, “Alternating Current Electrothermal Flow for Energy Efficient Thermal Management of Microprocessor Hotspot”, Applied Physics, 2018

[4] DanishAnsari, Kwang-YongKim, “Hotspot thermal management using a microchannel-pinfin hybrid heat sink”, International Journal of Thermal Sciences, Volume 134, December 2018, pp.27-39.

[5] G. J. Snyder, M. Soto, et al., "Hotspot cooling using embedded thermoelectric coolers," 22nd Annual IEEE Semiconductor Thermal Measurement And Management Symposium, Dallas, TX, 2006, pp. 135-143.

[6] G Bindiganavale, et al., “Study of hotspot cooling using electrowetting on dielectric digital microfluidic system”, 2014 IEEE 27th International Conference on Micro Electro Mechanical Systems (MEMS), San Francisco, CA, 2014, pp. 1039-1042.

[7] T.-W. Wei, H. Oprins, et al., "High efficiency direct liquid jet impingement cooling of high power devices using a 3D-shaped polymer cooler," 2017 IEEE International Electron Devices Meeting (IEDM), San Francisco, CA, 2017, pp. 32.5.1-32.5.4.

[8] Tiwei Wei, Herman Oprins, et al., “Experimental characterization and model validation of liquid jet impingement cooling using a high spatial resolution and programmable thermal test chip”, Applied thermal engineering, 2019, *submitted*.

[9] T.-W. Wei, H. Oprins, et al., "3D Printed Liquid Jet Impingement Cooler: Demonstration, Opportunities and Challenges," 2018 IEEE 68th Electronic Components and Technology Conference (ECTC), San Diego, CA, 2018, pp. 2389-2396.

[10] H. Oprins, et al., “Characterization and Benchmarking of the Low Intertier Thermal Resistance of Three-Dimensional Hybrid Cu/Dielectric Wafer-to-Wafer Bonding”. ASME. J. Electron. Packag. 2017;139(1):011008-011008-9.

[11] Tiwei Wei, Herman Oprins, et al., “Nozzle array scaling analysis of the thermal performance of liquid jet impingement coolers for high performance electronic applications”, The International Heat Transfer Conferences (IHTC), 2018.